International Journal of Engineering, Mathematical and Physical Sciences
ISSN: 2517-9934
Vol:6, No:4, 2012

Fault Detection of Pipeline in Water Distribution Network System

Shin Je Lee, Go Bong Choi, Jeong Cheol Seo, Jong Min Lee and Gibaek Lee

Abstract—Water pipe network is installed underground and once equipped, it is difficult to recognize the state of pipes when the leak or burst happens. Accordingly, post management is often delayed after the fault occurs. Therefore, the systematic fault management system of water pipe network is required to prevent the accident and minimize the loss. In this work, we develop online fault detection system of water pipe network using data of pipes such as flow rate or pressure. The transient model describing water flow in pipelines is presented and simulated using MATLAB. The fault situations such as the leak or burst can be also simulated and flow rate or pressure data when the fault happens are collected. Faults are detected using statistical methods of fast Fourier transform and discrete wavelet transform, and they are compared to find which method shows the better fault detection performance.

Keywords—fault detection, water pipeline model, fast Fourier transform, discrete wavelet transform.

I. Introduction

WATER supply network is a large system to distribute water to house and industry. This network is installed underground and entangled complicatedly. Therefore, it is difficult to recognize faults such as leak or burst when the faults happen. Also, since the number of sensors to measure pressure or flow rate of the pipe is limited, accurate fault detection is hardly possible. As longer as the fault detection is delayed, economical and social losses are bigger and bigger. Thus, the detection techniques are required to minimize the massive loss when the faults occur. In this work, we develop a mathematical model of pipelines and simulate to collect the pressure and flow rate data when the leak is created. Then, we present the fault detection techniques, fast Fourier transform (FFT) and discrete wavelet transform (DWT) based on statistical methods. These techniques are applied to the simulated data with the leak to show the fault detection performance. We also apply the proposed detection schemes to real data obtained from a small area. This paper is organized follows. Section 2 shows the procedure of modeling of pipelines and simulation results. Then, fast Fourier transform and wavelet transform are mathematically explained at Section 3. Section 4 presents the results of fault detection with the simulated data and real data using the proposed methods. Finally, it is followed by Conclusion.

S. J. Lee, G. B. Choi and J. M. Lee are with the School of Chemical and Biological Engineering, Seoul National University, Seoul 151-744, South Korea.
J. C. Seo is with Samchully Corporation, Seoul 150-885, South Korea.
G. Lee is with the Department of Chemical and Biological Engineering, Korea National University of Transportation, Chungju, Chungbuk 380-720, South Korea.

II. Mathematical model

A. Model of Pipeline

Modeling transients in pipelines and pipe networks is presented by Wylie [1]. Unsteady state flow in a pipeline can be described by the principles of conservation of mass and momentum. The simplified continuity and motion equations are in the form of

$$\frac{\partial H}{\partial t} + V\frac{\partial H}{\partial x} + \frac{a^2}{gA}\frac{\partial Q}{\partial x} = 0 \tag{1}$$

$$\frac{1}{gA}\frac{\partial Q}{\partial t} + \frac{V}{gA}\frac{\partial Q}{\partial x} + \frac{\partial H}{\partial x} + \frac{fQ|Q|}{2gDA^2} = 0 \tag{2}$$

where H is hydraulic head, Q is volumetric flow rate, V is mean velocity of the flow, g is gravitational acceleration, a is wave speed in a conduit, f is friction factor, D is pipe diameter, A is cross-sectional area, x is distance along the pipe, and t is time. Wave speed can be calculated from

$$a = \sqrt{\frac{\frac{K}{\rho}}{1 + \frac{K}{E}\frac{D}{e}\phi}} \tag{3}$$

where K is bulk modulus of elasticity of the fluid, e is pipe wall thickness, E is Young's modulus of elasticity of the conduit walls, ρ is fluid density, and ϕ is parameter depending on the pipe anchoring. The transient model is partial differential equation (PDE) and it requires a particular solution scheme to convert the PDE to a set of ODEs.

B. Method of Characteristics

The method of characteristics (MOC) is one of the most popular techniques for solving the above partial differential equation [2]. The governing pipe flow equations are written as

$$L_1 = \frac{\partial H}{\partial t} + V\frac{\partial H}{\partial x} + \frac{a^2}{gA}\frac{\partial Q}{\partial x} = 0 \tag{4}$$

$$L_2 = \frac{1}{gA}\frac{\partial Q}{\partial t} + \frac{V}{gA}\frac{\partial Q}{\partial x} + \frac{\partial H}{\partial x} + \frac{fQ|Q|}{2gDA^2} = 0 \tag{5}$$

A linear combination of Equations (4) and (5) is derived as

$$\begin{aligned} \lambda L_1 + L_2 = \; & \tfrac{1}{gA}\left[\tfrac{\partial Q}{\partial t} + (V + \lambda a^2)\tfrac{\partial Q}{\partial x}\right] + \\ & \lambda\left[\tfrac{\partial H}{\partial t} + (V + \tfrac{1}{\lambda})\tfrac{\partial H}{\partial x}\right] + \tfrac{fQ|Q|}{2gDA^2} = 0 \end{aligned} \tag{6}$$

The time derivatives of Q and H are expressed as

$$\frac{dQ}{dt} = \frac{\partial Q}{\partial t} + \frac{dx}{dt}\frac{\partial Q}{\partial x} \tag{7}$$

$$\frac{dH}{dt} = \frac{\partial H}{\partial t} + \frac{dx}{dt}\frac{\partial H}{\partial x} \tag{8}$$

respectively. The time derivative of x can be derived as

$$\frac{dx}{dt} = V + \lambda a^2 = V + \frac{1}{\lambda} \tag{9}$$

comparing the bracketed terms of Equation (6) and Equations (7) and (8). Then, the PDE (6) is transformed to the ODE

$$\frac{1}{gA}\frac{dQ}{dt} + \lambda\frac{dH}{dt} + \frac{fQ|Q|}{2gDA^2} = 0 \tag{10}$$

From the second and third terms of Equation (9), the following is obtained

$$\lambda = \pm\frac{1}{a} \tag{11}$$

and using this, the time derivative of x reduces to

$$\frac{dx}{dt} = V \pm a \tag{12}$$

The flow velocity, V, can be neglected in water pipes, then Equation (12) becomes

$$\frac{dx}{dt} = \pm a \tag{13}$$

Equation (13) defines two straight lines, called characteristics. The characteristic associated with $+a$ is referred to as the C^+ characteristic, and the C^- characteristic is associated with $-a$. Substituting corresponding values of λ into Equation (10) leads to two pairs of equations which are identified as C^+ and C^-.

$$C^+ : \begin{cases} \frac{a}{gA}\frac{dQ}{dt} + \frac{dH}{dt} + \frac{fQ|Q|a}{2gDA^2} = 0 \\ \frac{dx}{dt} = +a \end{cases} \tag{14}$$

$$C^- : \begin{cases} \frac{a}{gA}\frac{dQ}{dt} - \frac{dH}{dt} + \frac{fQ|Q|a}{2gDA^2} = 0 \\ \frac{dx}{dt} = -a \end{cases} \tag{15}$$

Equations (14) and (15) are called compatiblity equations and used to solve for points in the xt plane. The solution of compatibility equations is achieved by integration using an approximation of the friction term (the third term on the left hand side). A linear approximation of the flow between end points gives

$$C^+ : \frac{a}{gA}(Q_P - Q_A) + (H_P - H_A) + \frac{f\Delta x}{2gDA^2}Q_P|Q_A| = 0 \tag{16}$$

$$C^- : \frac{a}{gA}(Q_P - Q_B) + (H_P - H_B) + \frac{f\Delta x}{2gDA^2}Q_P|Q_B| = 0 \tag{17}$$

The simultaneous solution of two compatibility equations yields the conditions at a particular time and position in the xt plane designated by point P, given the conditions at a previous time step (points A and B), as shown in Fig. 1. Solving for H_P simplifies Equations (16) and (17) to

$$C^+ : H_P = C_P - BQ_P \tag{18}$$

$$C^- : H_P = C_M + BQ_P \tag{19}$$

where C_P and C_M are constants defined at the previous step

$$C_P = H_A + Q_A(B - R|Q_A|) \tag{20}$$

$$C_M = H_B - Q_B(B - R|Q_B|) \tag{21}$$

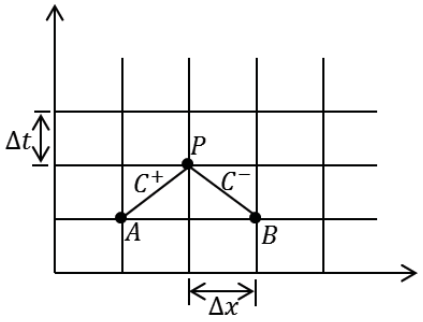

Fig. 1. Charateristics grid

B and R are written as

$$B = \frac{a}{gA} \tag{22}$$

$$R = \frac{f\Delta x}{2gDA^2} \tag{23}$$

respectively. H_P can be solved using Equations (18) and (19)

$$H_P = \frac{C_P + C_M}{2} \tag{24}$$

Q_P can then be calculated from Equation (18) or (19)

$$Q_P = \frac{C_P - H_P}{B} \tag{25}$$

$$Q_P = \frac{H_P - C_M}{B} \tag{26}$$

At ends of the single pipe, only one of the compatibility equations is available. Thus, the boundary conditions of the pipeline are used to specify Q_P or H_P at ends. The boundary equation for the leak is presented in the next section.

C. Leakage Boundary

An orifice equation that describes the leak has the following form

$$Q_L = C_d A_0 \sqrt{2gH_L} \tag{27}$$

where Q_L and H_L are the flow through the orifice and a hydraulic head at the leak, respectively, C_d and A_0 is an orifice discharge coefficient and the cross-section area of the orifice, respectivley. A mass balance equation for the leakage node is given as

$$Q_u - Q_d - Q_L = 0 \tag{28}$$

where Q_u and Q_d are the upstream and downstream flows, respectively, derived from Equations (25) and (26) with H_L instead of H_P. H_L can be found by substituting modified ones of Equations (25) and (26), and Equation (27) into Equation (28). Q_u and Q_d can then be obtained using H_L.

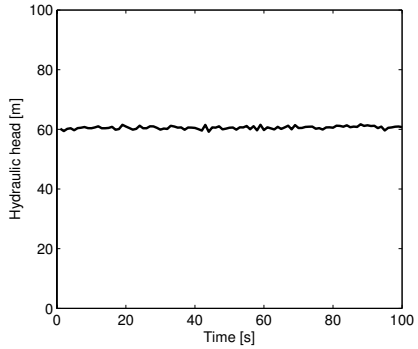

(a) No leak

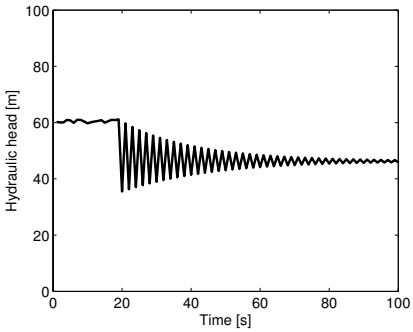

(b) Leak

Fig. 2. Hydraulic heads without leak (a) and with leak (b)

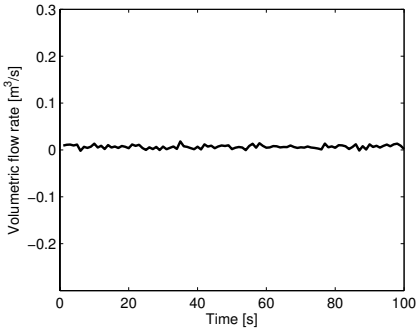

(a) No leak

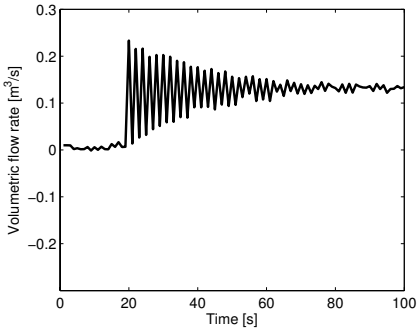

(b) Leak

Fig. 3. Volumetric flow rates without leak (a) and with leak (b)

D. Simulation Results

The simulation results from the presented transient model are shown. The pipe diameter is 1.22 m and the pipe length is 100 m discretized by 1 so that it has 100 points. The simulation is implemented for 100 s. Eventually, it has 10000 nodes in the xt plane. We show the hydraulic head and volumetric flow rate of the single pipe when having the leak or not. The leak happens on 30 m point of the pipe at 20 s. Fig. 2 shows the hydraulic heads without the leak and with the leak. When the leak occurs, the hydraulic head drops about 20 m and converges on 46 m. Fig. 3 shows the volumetric flow rates of cases without the leak and with the leak. The volumetric flow rate rises to 0.2 m^3/s and converges to 0.14 m^3/s.

III. Fault detection techniques

We here present the fault detection techniques, fast Fourier transform (FFT) and wavelet transform (WT). The mathematical algorithms of these methods are explained in this section.

A. Fast Fourier Transform

The Fourier transform is a reversible, linear transform with many important properties. For any function $f(t)$, the Fourier transform can be denoted $F(s)$, where $f(t)$ is the time-domain signal and $F(s)$ is the frequency-domain signal. The Fourier transform is defined by

$$F(s) = \int_{-\infty}^{\infty} f(t)e^{-2\pi ist}dt, \quad i = \sqrt{-1} \tag{29}$$

The continuous Fourier transform (CFT) converts a time-domain signal of infinite duration into a continuous spectrum composed of an infinite number of sinusiods. We usually deal with signals that are discretely sampled at constant intervals and of finite furation. Only a finite number of sinusoids is needed for such data and the discrete Fourier transform (DFT) is appropiate. The DFT of N uniformly sampled data points x_n (where $n = 0, \cdots, N-1$) is defined by

$$X_k = \sum_{n=0}^{N-1} x_n e^{-2\pi ink/N}, \quad k = 0, \cdots, N-1 \tag{30}$$

The continuous variable s is replaced by the discrete variable k. The DFT is usually computed by an efficient algorithm known as the fast Fourier transform (FFT). The key advantage of the FFT over the DFT is that the operational complexity decreases from $O(N^2)$ for the DFT to $O(N \log_2 N)$ for the FFT. When comparing the speeds obtained by computing the FFTs and DFTs for length 10^3 and 10^6 points, the difference

is quite clear.

$$\text{speed improvement} \quad (N = 10^3) \propto \frac{N^2}{N \log_2 N} \approx \frac{10^3}{10} \approx 10^2 \tag{31}$$

$$\text{speed improvement} \quad (N = 10^6) \propto \frac{N^2}{N \log_2 N} \approx \frac{10^6}{20} \approx 5 \times 10^4 \tag{32}$$

We can notice the fault by comparing the spectrum of original signals using the FFT [4].

B. Wavelet Transform

The wavelet transform (WT) decomposes a given signal into its frequncey components like the Fourier transform, but differes in giving a global representation of the signal. The WT provides a representation in both time and frequency. A mathematical definition of the continuous wavelet transform (CWT) follows [4]

$$CWT_\Psi f(a,b) = |a|^{-1/2} \int_{-\infty}^{\infty} f(t) \Psi^* \left(\frac{t-b}{a} \right) dt \tag{33}$$

where $\Psi(t)$ is the mother wavelet and a and b are dilating and translating coefficients, respectively. The asterisk denotes a complex conjugate and the multiplication of $|a|^{-1/2}$ is for energy normalization. The WT decomposes the signal into different scales with different levels of resolution by dilating the mother wavelet. One drawback of the CWT is that the representation of the siganl is redundant, since a and b are continuous over $\mathbf{R}$ where $\mathbf{R}$ is the set of real numbers. A discrete wavelet function (DWT) solves the drawback [3]. A wavelet function $\psi(t) \in L^2(\mathbf{R})$ has the following basic properties

$$\int_{\mathbf{R}} \psi(t) dt = 0 \quad \text{and} \quad \int_{\mathbf{R}} \psi^2(t) dt = 1 \tag{34}$$

We also require a scaling function $\phi \in L^2(\mathbf{R})$ that satisfies

$$\int_{\mathbf{R}} \phi(t) dt \neq 0 \quad \text{and} \quad \int_{\mathbf{R}} \phi^2(t) dt = 1 \tag{35}$$

Let $\mathbf{Z}$ denote the set of all integers. Starting from choices of $\phi(t)$ and $\psi(t)$ and using dilations of $\eta = 2^{j_0}$ and $\eta = 2^j$ with translations of $\tau = k$ for $j_0, j, k \in \mathbf{Z}$, we can construct an orthonormal basis for the space $L^2(\mathbf{R})$ consisting of the scaling functions $\left\{\phi_{j_0,k}(t) = 2^{j_0/2}\phi(2^{j_0}t - k)\right\}$ and the wavelet functions $\left\{\psi_{j,k}(t) = 2^{j/2}\psi(2^j t - k)\right\}$. Then, any target function $f(t)$ can be expressed as

$$f(t) = \sum_{k \in \mathbf{Z}} c_{j_0} \phi j_0, k(t) + \sum_{j=j_0}^{\infty} \sum_{k \in \mathbf{Z}} d_{j,k} \phi_{j,k}(t) \tag{36}$$

where the coefficients

$$c_{j_0,k} = \int_{\mathbf{R}} f(t) \phi_{j_0,k}(t) dt \tag{37}$$

$$d_{j,k} = \int_{\mathbf{R}} f(t) \psi_{j,k}(t) dt \tag{38}$$

are defined as the inner product of $f(t)$ with the basis functions $\phi_{j_0,k}(t)$ and $\psi_{j,k}(t)$, respectively, and called approximation coefficients and detailed coefficients, respectively. When DWT is applied to a data set of N, the DWT transforms N data points into N wavelet coefficients. The original data can be expressed as a linear sum of products of wavelet coefficients and their corresponding basis functions, as in Equation (36). Daubechies' wavelet, Morlet wavelet, and Harr wavelet are popularly used for the wavelet and scaling functions. The DWT can be used to detect the fault by observing the wavelet coefficients [5].

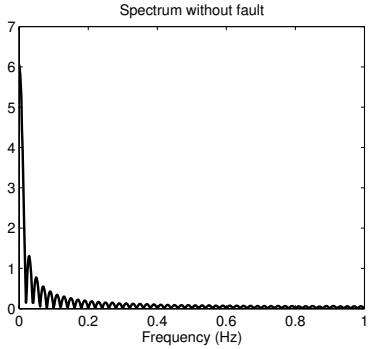

Fig. 4. FFT of hydraulic head without fault

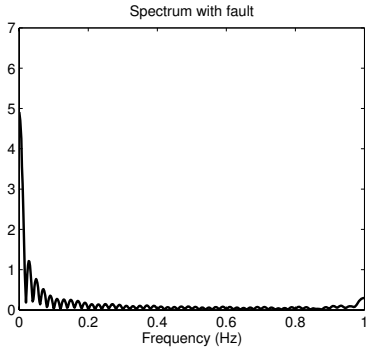

Fig. 5. FFT of hydraulic head with fault

IV. Results and Discussion

We present the results of fault detection using the proposed detection schemes, the FFT and the DWT. We first apply the techniques to the simulated data shown in Section 2. Real data of pressure of pipe network are also used to detect faults to show that the presented schemes work well for actual situations.

A. Fault Detection with Simulated Data

We first compare the spertrum of the simulated hydraulic heads without and with the fault using the FFT. The spectrum are shown in Fig. 4 and Fig. 5. The spectrum with the fault differ from the one without the fault around 0 Hz and 1 Hz. The faults can be noticed by comparing the spectrum of original signals, however, it does not give any information about the time of the fault. Now we present the results of the DWTs of the simulated hydraulic heads without and with the fault as shown in Fig. 6 and Fig. 7. When the pipeline has

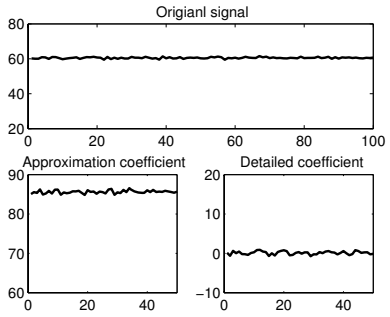

Fig. 6. DWT of hydraulic head without fault

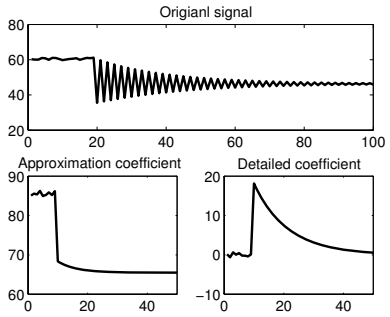

Fig. 7. DWT of hydraulic head with fault

the fault, the wavelet coefficients are changed sharply as in Fig. 7. Thus, the faults are easily recognized by observing the wavelet coefficients. In addition, the DWT gives information about the time of the fault. The simulated fault happens at 20 s and the wavelet coefficients change rapidly about 10 s because of the Nyqyust frequency. We can estimate the time of the fault using this information.

B. Fault Detection with Real Data

Fig. 8 shows pressure changes of Area S for Day 1 and Day 2. The pressure is measured every minutes for 24 hours, thus, it has the total data points of 1440. We can infer a severe fault for Day 2 from the fact that the pressure at 600 s drops rapidly and goes zero after 1100 s. The FFTs of pressure data are shown in Fig. 9. The spectrum of pressures for Day 1 and Day 2 are different each other around 0 Hz. Although the difference of the spectrum is recognized, it is not clear to detect the serious fault. Now we apply the DWT to the pressure data and obtain results as shown in Fig. 10 and Fig. 11. The fault detection of the DWT is quite obvious by observing detailed coefficients for Day 1 and Day 2. Peaks in the detailed coefficient for Day 2 represent the faults of the pipe at 600 s and 1100 s, noting that the time scale is scaled down the half of the whole duration due to the Nyquist frequency.

V. Conclusion

In this work, we propose fault detection techniques, the fast Fourier transform and the discrete wavelet transform, for the

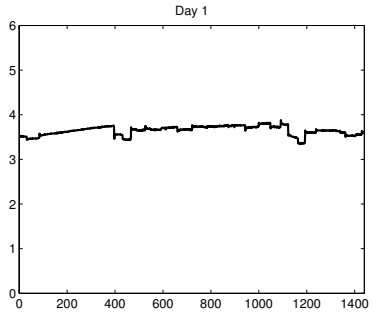

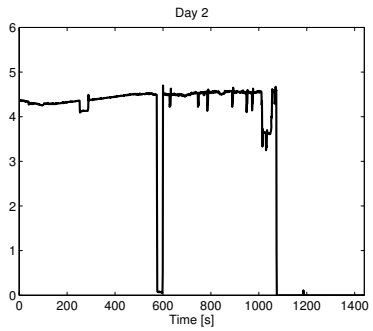

Fig. 8. Pressure changes of Area S for Day 1 and Day 2

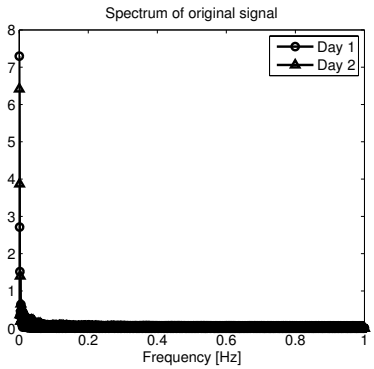

Fig. 9. FFTs of pressures of Area S

water pipe network system. First of all, the transient model for the pipeline is developed and simulated to collect the data of the hydraulic head and volumetric flow rate of the pipe when the fault is generated. The presented detection techniques show good performance by detecting the fault. In general, the DWT shows better performance than the FFT. These schemes are also applied to real data obtained from Area S for two days, resulting in good detection performance for the faults occured on Day 2.

Acknowledgment

This work is supported by Korean Ministry of Environment as Projects for Developing Eco-Innovation Technologies (GT-

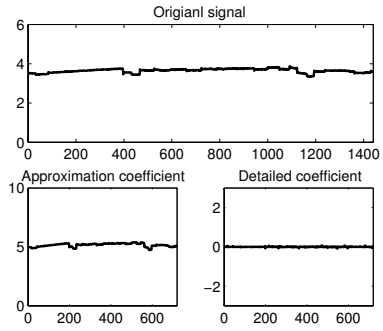

Fig. 10. DWT of pressure of Area S for Day 1

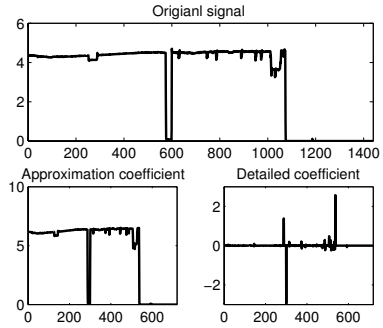

Fig. 11. DWT of pressue of Area S for Day 2

11-G-02-001-3).

REFERENCES

[1] E. B. Wylie, "The Microcomputer and Pipeline Transients", *Journal of Hydraulic Engineering*, vol. 109, no. 12, pp. 1723-1739, 1983.
[2] D. Misiunas, *Failure Monitoring and Asset Condition Assessment in Water Supply Systems*, Lund Univ., 1999.
[3] E.K. Lada, J. C. Lu, and J. R. Wilson, "A Wavelet-Based Procedure for Process Fault Detection", *IEEE Transactions on Semiconductor Manufacturing*, vol. 15, no. 1, pp. 79-90, 2002.
[4] L. Satish, "Short-time Fourier and Wavelet Transforms for Fault Detection in Power Transformers during Impulse Tests", *IEE Proc.-Sci. Meas. Technol.*, vol. 145, no. 2, pp. 77-84, 1998.
[5] S. Bhunia, K. Roy, and J. Segura, "A Novel Wavelet Transform Based Transient Current Analysis for Fault Detection and Localization", *DAC*, vol. 25, no. 2, pp. 361-366, 2002.

Shin Je Lee received the B.S degree in chemical and biomolecular engineering from Sogang University, Seoul, South Korea in 2011. She is working toward the M.S. degree in chemical and biological engineering at Seoul National University, Seoul, South Korea.

Go Bong Choi received the B.S degree in chemical and biological engineering from Seoul National University, Seoul, South Korea in 2011. He is working toward Ph.D. degree in chemical and biological engineering at Seoul National University, Seoul, South Korea.

Jeong Cheol Seo received the B.S, M.S., and Ph.D. degrees in chemical engineering from Seoul National University, Seoul, South Korea in 1991, 1993, and 1997, respectively. He is currently a director of Samchully Corporation, Seoul, South Korea.

Jong Min Lee received the B.S degree in chemical engineering from Seoul National University, Seoul, South Korea in 1996 and the Ph.D. degree in chemical and biomolecular engineering form the Georgia Institute of Technology in 2004, Atlanta. He is currently an assistant professor of the School of Chemical and Biological Engineering at Seoul National University, Seoul, South Korea.

Gibaek Lee received the B.S, M.S., and Ph.D. degrees in chemical engineering from Seoul National University, Seoul, South Korea in 1991, 1993, and 1997, respectively. He is currently a professor of the Department of Chemical and Biological Engineering, Korea National University of Transportation, Chungju, South Korea.